metals

MDPI

Article

Optimization of Si Content to Inhibit Inhomogeneous Deformation in Al-Mg-Si Alloy Fabricated via Twin-Roll Casting

Bowen Wei [1,2], Shiju Li [1], Tao Jiang [1], Youyun Zhang [1], Guangming Xu [1,*], Yong Li [2,*] and Zhaodong Wang [2]

[1] Key Laboratory of Electromagnetic Processing of Materials of Ministry of Education, Northeastern University, Shenyang 110819, China; 1610210@stu.neu.edu.cn (B.W.); 1710221@stu.neu.edu.cn (S.L.); 1710193@stu.neu.edu.cn (T.J.); 1910129@stu.neu.edu.cn (Y.Z.)

[2] State Key Laboratory of Rolling and Automation, Northeastern University, Shenyang 110819, China; zhdwang@mail.neu.edu.cn

* Correspondence: xu_gm@epm.neu.edu.cn (G.X.); liyong@ral.neu.edu.cn (Y.L.); Tel.: +86-133-0404-9003 (G.X.); +86-180-4025-9960 (Y.L.)

Abstract: Herein, the effects of Si content on the microstructure evolution of Al-Mg-Si alloys during twin-roll casting (TRC) and subsequent heat treatment were characterized using scanning electron microscopy, emission electron probe micro analysis, electron backscatter diffraction, and transmission electron microscopy. The effects of insoluble Si particles, solute gradient, and recrystallization on the mechanical properties of the alloy in the T4P state were analyzed. An inhomogeneous deformation in the thickness direction of the TRC strip was observed during the pre-strain test. A premature local deformation at the element barren region (EBR) in the middle of the strip was considered to be the origin of the limited mechanical properties. By increasing the Si from 0.7 wt% to 1.1 wt%, the content and uniformity of the solute in the EBR can be effectively improved. The stronger work-hardening ability weakens the inhomogeneous deformation. Si addition significantly increased the number of insoluble Si particles during the heat treatment. The structure with a hard shell and soft core in the TRC strip significantly reduced the negative effect of insoluble Si particles on the mechanical properties. The tensile strength and uniform elongation of the strip increased from 159.44 MPa and 18.36% to 209.96 MPa and 29.791%, respectively.

Keywords: Al-Mg-Si alloy; twin-roll casting; silicon; inhomogeneous deformation; mechanical properties

Citation: Wei, B.; Li, S.; Jiang, T.; Zhang, Y.; Xu, G.; Li, Y.; Wang, Z. Optimization of Si Content to Inhibit Inhomogeneous Deformation in Al-Mg-Si Alloy Fabricated via Twin-Roll Casting. *Metals* **2022**, *12*, 941. https://doi.org/10.3390/met12060941

Academic Editors: Jingwei Zhao, Zhengyi Jiang, Leszek Adam Dobrzański and Chong Soo Lee

Received: 6 May 2022
Accepted: 28 May 2022
Published: 30 May 2022

1. Introduction

Al-Mg-Si alloys have the advantages of low weight, high strength, and high ductility, and are widely used in automobile sheet manufacturing [1,2]. Currently, the production process of automobile plates includes direct-chilling casting (DC), hot rolling, cold rolling, solution, quenching, pre-aging, and bake hardening. In this process, an alloy in the T4P state (pre-aging after solution) with excellent ductility is used for forming, and the β″ precipitates that are precipitated during bake hardening are used to improve the strength. To improve the surface quality and uniformity of the solution elements, casting billets are processed by cogging, surface milling, and long-term homogenization. However, this process is cumbersome and expensive.

In recent years, sub-rapid solidification technology has attracted increasing attention because it can improve the material properties and simplify the processing. Common sub-rapid solidification techniques include twin-roll casting (TRC), spray forming, and die casting. As a thin strip production process, TRC is suitable for automobile sheet production. In this process, the metal melt is directly injected to the gap between two rotating water-cooled metal rolls, and the solidification and rolling processes are completed simultaneously to obtain a strip with fine grains and no porosity directly during

the TRC process [3]. However, obvious macrosegregation was observed in the alloys produced by TRC [4,5]. The homogenization of alloys to improve their properties is the traditional material-optimization approach. Many researchers have attempted to eliminate macrosegregation by optimizing the TRC process. Haga et al. focused on a high-speed TRC route to obtain an alloy with fine grains and high solid solubility to eliminate centerline segregation [6]. In recent years, research has been conducted on the influence of external fields on the solute distribution during TRC, and it was reported that an oscillating electromagnetic field significantly reduces the degree of macro-and micro-segregation [7–9]. However, these process optimization methods significantly increase the production costs.

With further research on the microstructure of TRC alloys, the design of alloy composition systems that are more suitable for the TRC process has been another popular research direction. The composition design of Al-Mg-Si alloys has been studied in depth [10–12]. The morphology of the branch crystal, element distribution, and second phase of the alloy prepared by TRC differ significantly from those prepared by direct-chilling casting. The composition design of the Al-Mg-Si alloy fabricated by TRC has seen renewed interest. Liu et al. found that the formation of the α-AlFeSi phase is promoted by increasing the Mg content during sub-rapid solidification [13]. Liu et al. found that π-AlFeMgSi in TRC samples expands the solubility range of the solid solution and promotes aging precipitation [14]. Wang et al. reduced the centerline segregation area of the Al-Mg-Si alloy prepared by TRC by adding Cr, thereby decreasing the yield strength of the T4 alloy and improving the strength and elongation of the T6 alloy [15]. However, the effect of Si on the mechanical properties of Al-Mg-Si alloys prepared by TRC has not yet been reported.

In this study, the microstructural evolution of Al-Mg-Si alloys with different Si contents during TRC and subsequent processing was characterized. The effect of the Si content on the mechanical properties of the alloy was analyzed. The inhomogeneous deformation in the middle of the strip was weakened by optimizing the Si content. Both the strength and uniform elongation of the strip improved. The obtained results can be used to optimize the composition design of the Al-Mg-Si alloys fabricated for automotive strips using TRC.

2. Experimental Procedure

An Al-Mg-Si alloy strip was prepared using a vertical TRC machine (NEU, Shenyang, China) with a roll diameter of 360 mm developed by our laboratory. According to the amount of added Si, the experimental subjects were divided into 5 groups with Si contents of 0.7, 0.9, 1.1, 1.3 and 1.5 wt%, respectively. The contents of other alloying elements were the same, and the alloy contained 0.5 wt% Mg, 0.1 wt% Mn, and 0.1 wt% Cu with Al balance. To prepare the strip, commercial 99.99% aluminum ingots, and Al-50Mg, Al-20Si, Al-10Mn, and Al-50Cu alloys were melted in an industrial resistance furnace (GEF, Shenyang, China) and maintained at 750 °C for 1 h. Prior to casting, the melt temperature was reduced to 710 °C and 0.4 wt% Al-5Ti-B was added as the grain refiner. Before casting, the roll gap was 0 mm, and a specific roll separating force of 1 kN/mm was applied. With the influx of melt, the roll gap was separated by the solidification shell and gradually approached a certain roll gap size. When the roller gap size fluctuation was very small, the position of the roller was fixed. The length of the tip set-back was 90 mm. The casting speed was 2.5 m·min^{-1}, and the strip width was 100 mm. Because Si content affects the solidification range of the alloy, the volume of the semi-solid melt at the kissing point is different with different Si content, which changes the average deformation resistance of the solidified shell. Under the condition of the same roll separating force, the thicknesses of the strips are slightly different, and their floating range is 5.04~5.16 mm. The actual elemental content of the strip was detected by X-ray fluorescence (XRF, ZSXPrimus II, Rigaku, Tokyo, Japan), and the results are shown in Table 1. After homogenization at 550 °C for 20 h, the TRC strip was cold-rolled from a thickness of approximately 5 mm to 1 mm. The cold-rolled strips were then subjected to solid-solution heat treatment at 565 °C for 20 min, water quenching, and pre-aging heat treatment at 150 °C for 8 min.

Table 1. Chemical compositions of the strips.

Mass Percentage (%)						
Si (Additive Amount)	**Al**	**Mg**	**Si**	**Fe**	**Mn**	**Cu**
0.7	97.87	0.516	0.685	0.121	0.093	0.089
0.9	97.82	0.505	0.892	0.133	0.085	0.103
1.1	97.55	0.498	1.107	0.142	0.108	0.097
1.3	97.24	0.491	1.318	0.138	0.102	0.113
1.5	97.03	0.509	1.473	0.147	0.097	0.107

The morphology of the second phase during TRC and subsequent processing was observed by scanning electron microscopy (SEM, ULTRA PLUS, Zeiss, Oberkochen, Germany) and optical microscopy (OM, BX53, OLYMPUS, Tokyo, Japan). The samples in the casting and T4P states (solid-solution and pre-aging heat treatment) were etched using Keller's reagent for 5 s. Because it was difficult to distinguish the insoluble particles from the Al matrix after homogenization by SEM, the samples were etched with a 20% NaOH solution at 80 °C for 20 s to obtain deeper etching. The content and elemental distribution of the second phase were analyzed using the energy-dispersive spectroscopy (EDS) module of the SEM. The precipitates of the strips in the T4P state were observed and qualitatively analyzed by transmission electron microscopy (TEM, Tecnai G2 F20, FEI, Hillsborough, OR, USA) and EDS. TEM thin foils were prepared by twinjet electropolishing using an electrolyte consisting of 10% perchloric acid and 90% methanol. The voltage was 15 V, and the polishing temperature was −25 °C. To characterize the macroscopic distribution of the solute elements in the strip, an emission electron probe microanalyzer (EPMA, JXA-8530F, JEOL, Akishima, Japan) was used to perform line scanning on the longitudinal section of the sample along the thickness direction. The samples used for EPMA were unetched. Electron backscatter diffraction (EBSD) was used to analyze the grain morphology, degree of deformation, and grain boundary distribution of the samples using a focused ion beam field-emission scanning electron microscope (FIB-SEM, crossbeam550, Zeiss, Oberkochen, Germany). Inverse pole figures (IPF), kernel average misorientation maps (KAM), and grain boundary (GB) distribution maps were calculated using Channel 5 software (5.11.20405.0, Oxford instruments, Abingdon, UK). To prepare the EBSD samples, a longitudinal section was selected as the observation plane. The plane was first polished with sandpaper, and then electropolished with a solution of 10% perchloric acid and 90% ethanol. The voltage was 25 V, and the polishing time was 30 s. The strip hardness was measured using an FM-700 Vickers hardness tester. The uniaxial tensile test was performed on an universal testing machine (CMT5105, SANS, Shenzhen, China) at 20 °C, with an initial strain rate of 1×10^{-3} s^{-1}. The average of the measured data of the three tensile specimens was used to analyze the performance of the strip. The length and width of the parallel section of the tensile specimen were 60 mm and 12.5 mm, respectively, and the gauge length was 50 mm. The fracture morphologies of the tensile samples were observed using a SEM (FEI QUANTA 600, FEI, Eindhoven, Netherlands).

3. Results

3.1. Second Phase

It is generally believed that the morphology and distribution of the intercrystalline eutectic phases should be controlled in terms of size and form as much as possible during the casting stage. This is because the subsequent rolling and heat treatment only have a limited effect on the microstructure. Compared with DC, the eutectic phase of the solidification structure during TRC is usually distributed at the triangular GB in near-surface regions with a large size, as shown in Figure 1a. The eutectic region presented a multiphase mixing state. A is the β-Al_5FeSi phase that absorbs Mn and begins to transform into the α-type, and is characterized by a semicircular protrusion at the short rod end. B is a short rod-like β-Al_5FeSi phase with bright linear fringes that correspond to the Cu

concentration area. These two phases have been thoroughly studied [16–18] and will not be discussed further in this paper. Map scanning shows Mg and Si in the C and D areas. Area C had a high Mg concentration and low Si concentration, whereas area D had a low Mg concentration and high Si concentration. According to the EDS results, C is the binary eutectic phase of Al + Mg_2Si and D is the ternary eutectic phase of Al + Mg_2Si + Si. The spot-like accumulation of Si in the D region was observed in the scanning map. The ternary eutectic phase has attracted our attention because it occupies a large proportion of the eutectic region and is widely distributed at triangular grain boundaries. This feature does not appear in alloys with similar compositions during DC or horizontal TRC [19]. The large eutectic phase strongly hinders the subsequent heat treatment process. As shown in Figure 1b, after homogenization, in addition to the insoluble β-Al_5FeSi phase, a large number of Si particles remained at the GB, as can be easily identified from the element scanning map. Because the Si content around the eutectic phase reached saturation, these Si particles can hardly dissolve in Al.

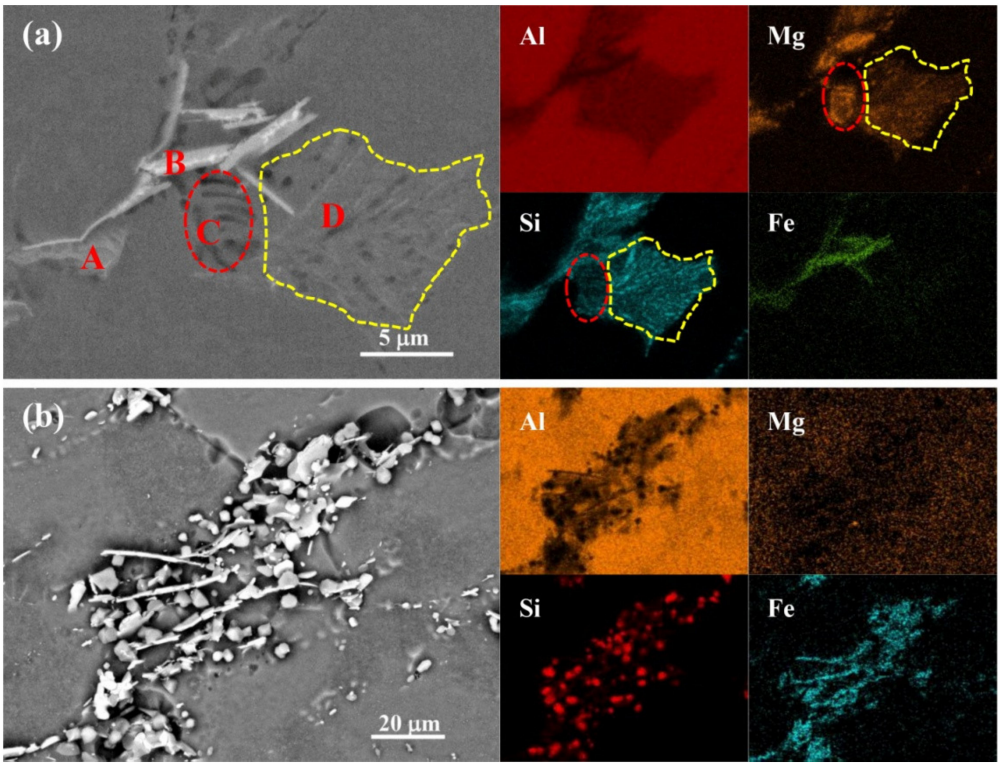

Figure 1. Eutectic phase morphology and element distribution in near-surface regions: (**a**) TRC strip; (**b**) TRC strip after homogenization.

Si phase and rod-like β-Al_5FeSi phase still exist in the T4P state strip, and their morphologies are respectively shown in circles A and B in Figure 2a. After cold rolling, the insoluble phases are further broken and their size decreases, reaching 2 μm. Furthermore, TEM was used to observe the precipitates in the grains, as shown in Figure 2b,c. The α-Al_5(FeMn)Si (circle C) exists generally in the matrix, but the quantity is small. The presence of β′ phase (point D) was found in only a few regions. Both precipitates were formed during homogenization [20]. Because the aging time was too short, no β″ precipitates were observed in all the TRC strips with different Si contents. These results are consistent with those obtained for the strips prepared from DC ingots [21].

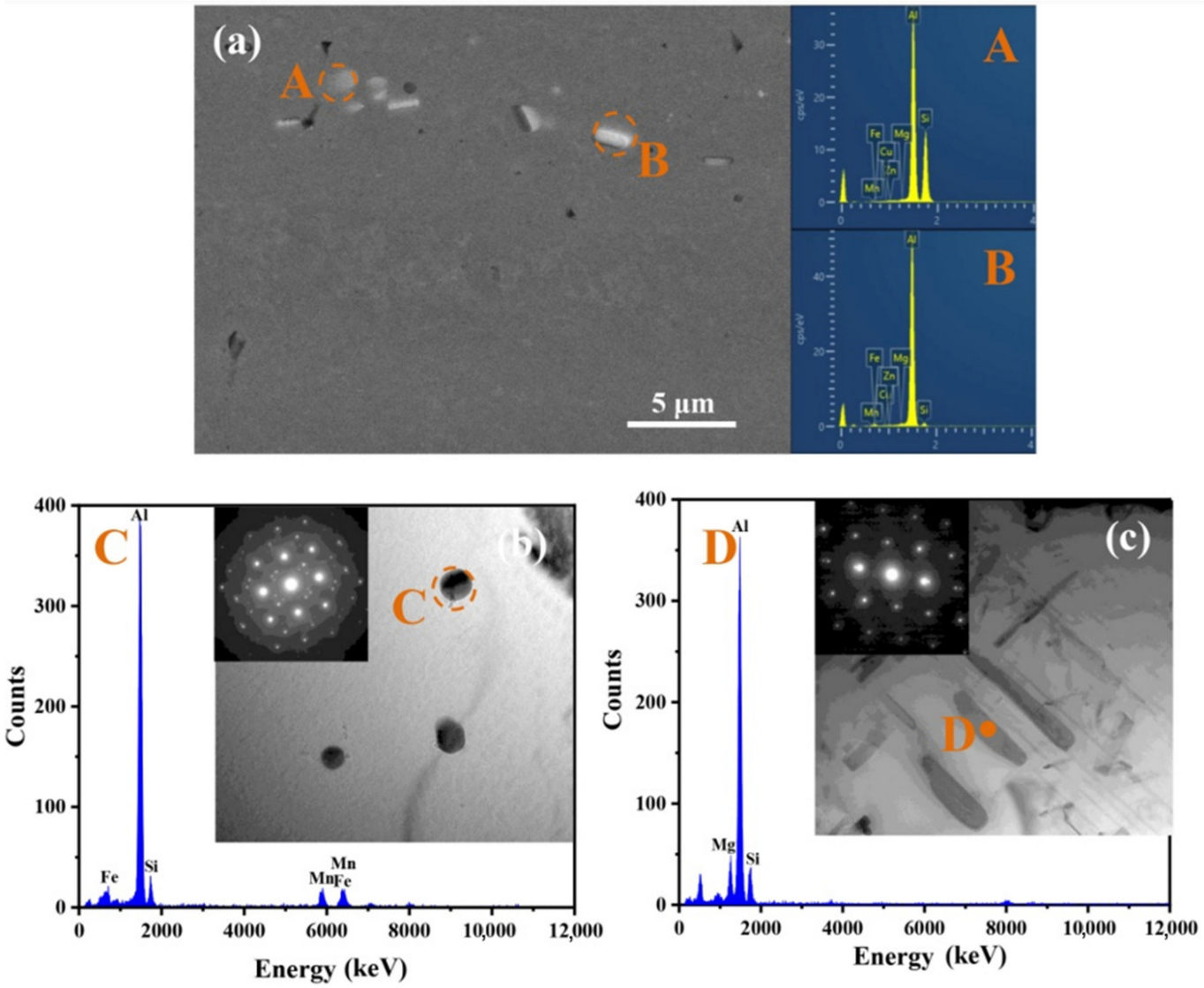

Figure 2. Second phase of the strips in the T4P state: (**a**) insoluble phase; (**b**) α-Al_5(FeMn)Si phase; (**c**) β′ phase.

According to the order of eutectic phase formation in the Al-Mg-Si alloys, a ternary eutectic phase can only be formed when Si is extremely enriched [22]. Therefore, adjusting only the amount of added Si without changing the contents of other alloying elements can significantly affect the number of residual particles at the grain boundaries after homogenization. Due to the effect of negative solute gradient in the thickness direction (discussed in Section 4.1), residual particles were mainly distributed on the surface region of the strip. Figure 3 shows the distribution of Si particles in the near-surface region of homogenized TRC strips with different Si contents and the morphology of residual Si particles. When the mass fractions of Si were 0.7% and 0.9%, there were fewer insoluble particles in the grain boundaries and the particles were generally distributed in the form of strips. When the mass fraction of Si was 1.1% or higher, the number of insoluble phases in the grain boundaries increased significantly, and local aggregation appeared.

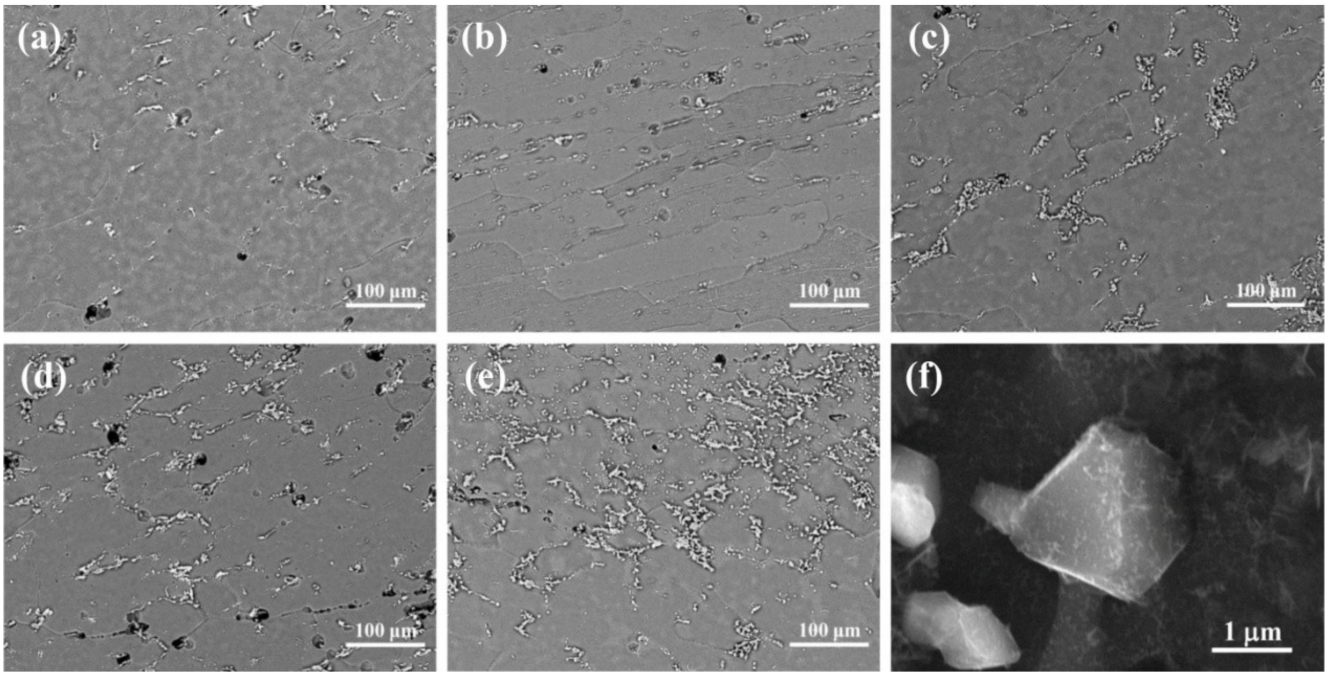

Figure 3. Distribution of Si particles in near-surface regions of homogenized TRC strips with different contents of Si: (**a**) 0.7 wt%; (**b**) 0.9 wt%; (**c**) 1.1 wt%; (**d**) 1.3 wt%; (**e**) 1.5 wt%; and (**f**) Si particle morphology.

3.2. Solute Gradient

A solute gradient is always observed in the vertical twin-roll casting (VTRC) strip. While the degree of microsegregation can be weakened during the subsequent heat treatment, the solute gradient at the macroscopic scale cannot be completely eliminated, significantly affecting the mechanical properties of the strip. EPMA was used to carry out line scanning on the longitudinal section of the strips along the thickness direction (for each strip, the thickness was 1 mm). The concentration gradients of Mg and Si are shown in Figure 4a and 4b respectively. To compare the solute gradients of the different strips, the average value of every 100 data points was calculated, and the average values are connected by straight lines. The results of Mg and Si are shown in Figure 4c and 4d respectively. The Mg and Si elements in all of the samples showed a negative solute gradient from the surface to the core regions of the strips. Grydin and Liu et al. found a similar phenomenon in VTRC strips, but did not carry out an in-depth analysis of its formation mechanism [23,24]. The negative solute gradient was generated in the strip during the TRC process, and its formation mechanism is analyzed in detail in Section 4.1. In addition, an element-positive segregation region with two surrounding elemental barren regions (EBRs) was found at the core regions of the strip. The amount of the elements added to the Al-Mg-Si alloy is generally low. EBRs have a greater impact on the mechanical properties because the alloying composition of the region is closer to that of pure aluminum, and the strain-hardening capacity is significantly reduced. The five groups of samples had similar contents of soluble Mg in the EBRs. The amount of soluble Si in the Al matrix increases with the thickness in any region when increasing the amount of added Si. When the Si content increased from 0.7 wt% to 1.1 wt%, the elemental content in the EBRs increased significantly.

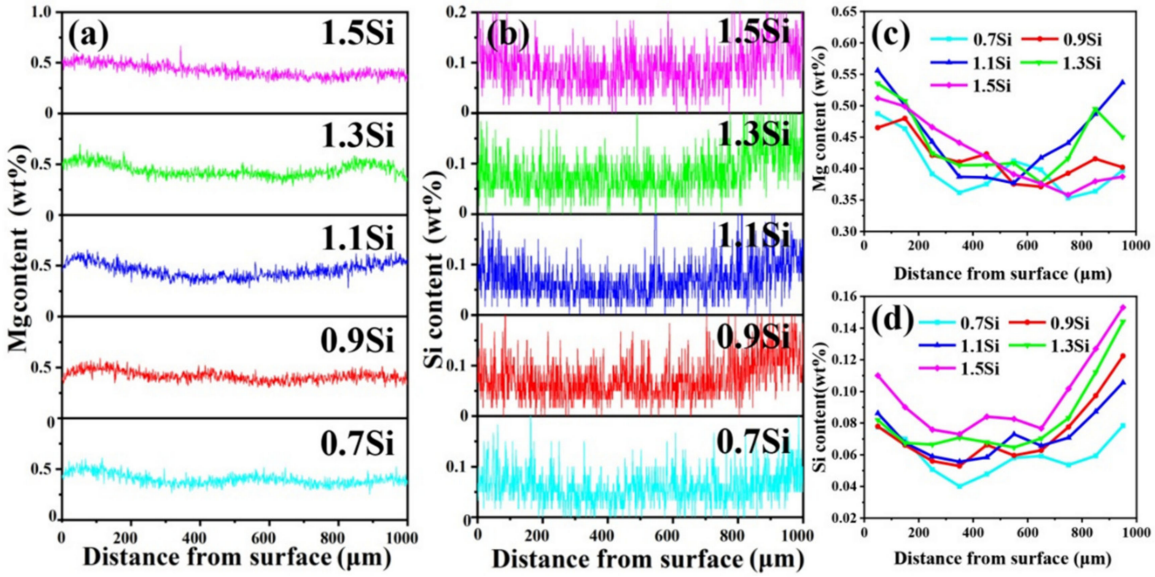

Figure 4. Solute gradient of the strips in the T4P state along the thickness direction; (**a**,**b**) the concentration gradients of Mg and Si; (**c**,**d**) average values.

3.3. Pre-Strain Test

To observe the strain distribution of the strips during deformation, a 12% pre-strain was applied to the strips with different Si contents in the T4P state. The pre-strain was performed using uniaxial tensile testing with an universal testing machine (CMT5105, SANS, Shenzhen, China) at 20 °C, and the initial strain rate was 1×10^{-3} s^{-1}. The microstructures of the samples were analyzed by EBSD. Due to the symmetry of the TRC structure in the thickness direction, only a half-thickness area was considered for observation, as shown in Figure 5. The upper and lower edges of the photograph represent the surface and core regions of the strip, respectively.

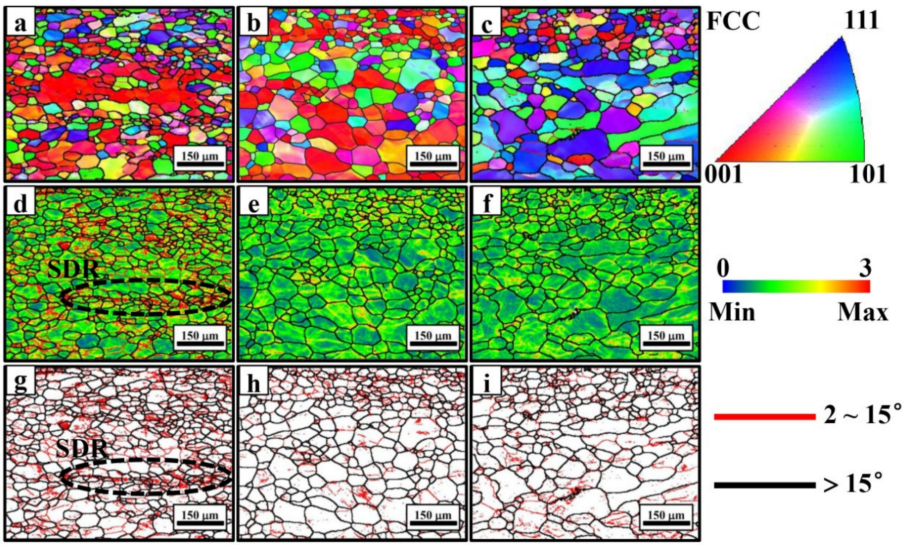

Figure 5. Grain morphologies and deformation characteristics of the strips obtained from the EBSD scans and IPFs of strips with 0.7 wt% Si (**a**), 1.1 wt% Si (**b**) and 1.5 wt% Si (**c**). KAM maps of the strips with 0.7 wt% Si (**d**), 1.1 wt% Si (**e**) and 1.5 wt% Si (**f**). GB distribution of strips with 0.7 wt% Si (**g**), 1.1 wt% Si (**h**) and 1.5 wt% Si (**i**).

Due to the low strain rate and low experimental temperature in the pre-strain test, no new recrystallization occurred in the samples. Figure 5a–c show that the recrystallization

grain size characteristics are still observed for the TRC strips in the T4P state. For the Si mass fraction of 0.7%, the grain size from the surface to the middle of the strip was small, but incomplete recrystallization was observed in the area of 1/4 thickness. Fine and large grains were found in the surface and middle regions of the strips with 1.1 wt% Si and 1.5 wt% Si, respectively.

The initial deformation of the samples was analyzed by the KAM and GB distributions, as shown in Figure 5d–i. A larger local misorientation angle in the KAM map indicates larger deformation [25]. An obvious non-uniform deformation was found in the sample with 0.7 wt% Si. Local strong deformation is mainly distributed at the grain boundaries and even through the grains. A band of a strong deformation region (SDR) passed through multiple grains approximately 350 μm from the surface of the strip. When the deformation increased further, a crack generation region appeared. The starting point (the x-coordinate is 0) of the line scanning of the sample with 0.7 wt% Si in Figure 4 is the same position as the upper edge of Figure 5d. It can be seen from the two figures that the EBRs and the strong deformation band of the sample with 0.7 wt% Si are both approximately 350 μm away from the surface. It can be inferred that the strong deformation band is generated in the EBRs. The GB distribution map shows that low-angle GBs at a high density are generated in the strong deformation area. They were transformed from a large number of accumulated dislocations, providing favorable conditions for the formation of microcracks. By contrast, only a small number of low-angle GBs were found in the samples with 1.1 wt% and 1.5 wt% Si, indicating that the deformation was more evenly distributed in each grain.

3.4. Hardness and Tensile Properties

Figure 6 shows the hardness distribution of the longitudinal section of the strip in the T4P state along the thickness direction. The TRC strip has the characteristics of a hard shell and a soft core [26], and the strip in the T4P state still has this characteristic. With an increase in the Si content, hardness increased at all positions along the thickness direction, with the largest increase observed when the mass fraction of Si was increased from 0.7% to 0.9%. However, when the mass fraction of Si exceeded 1.1%, the effect of the hardness improvement was significantly reduced. This is because the excess Si is more commonly found in the form of insoluble Si particles in the alloy, and the increase in the Si content in the Al solid solution is limited.

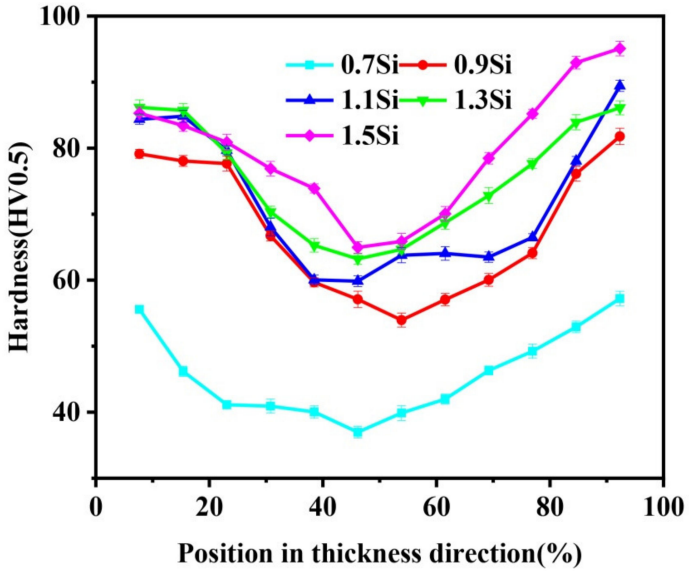

Figure 6. Hardness distribution of the strips in the thickness direction.

Figure 7 shows the engineering stress–strain curves of the strips. When the mass fraction of Si was increased from 0.7% to 1.1%, strength and ductility increased simultaneously.

The yield strength, tensile strength and uniform elongation increased from 67.51 MPa, 159.44 MPa and 18.36% to 93.185 MPa, 209.96 MPa, and 29.791%, respectively. With a further increase in the Si mass fraction from 1.1% to 1.5%, the tensile properties of the strip exhibited the opposite effects on strength and ductility. The strength increased slightly, but the elongation decreased significantly.

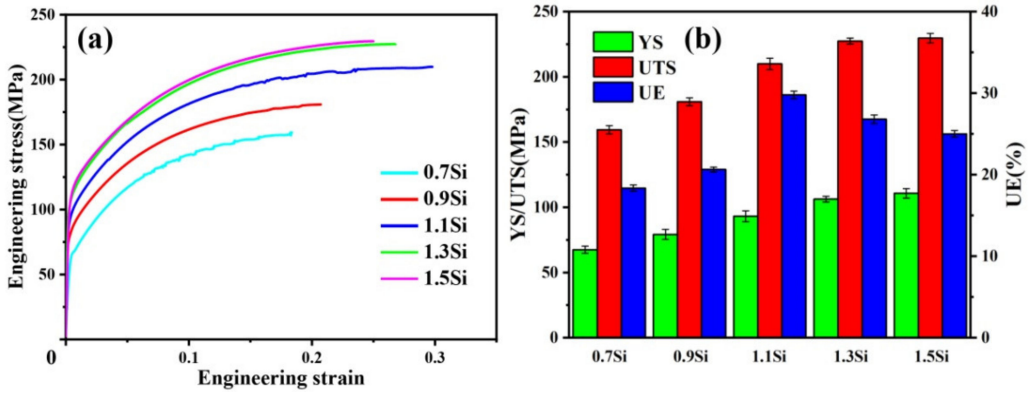

Figure 7. Tensile properties of the strips with different Si contents. (**a**) Engineering stress–strain curves. (**b**) Strength and uniform elongation.

3.5. Fracture Morphology

The tensile fractures observed in the middle region of the samples are shown in Figure 8. The fracture of the TRC strip in the T4P state was ductile fracture. In the middle region of the sample with 0.7 wt% Si, a wide range of planes was found. Because there is almost no precipitated phase or insoluble hard phase in the middle of the strip, the plane is the slip separation plane (SSP). The top edge of the plane had a ripple feature, below which an uncharacteristic extension zone was generated. EBRs with low work-hardening capacity and low sliding resistance led to the formation of SSPs during deformation. Some dimples at low depths were observed around the SSP. When the Si content increased to 0.9%, no large non-characteristic areas were observed, and more dimples were generated mixed with small SSP. The sample with the best ductility had a Si content of 1.1 wt%, and the middle region of the fracture was filled with a high number of large dimples. With an increase in the Si content to 1.5 wt%, the dimple size decreased, which was fully consistent with the variation in the tensile properties of the samples.

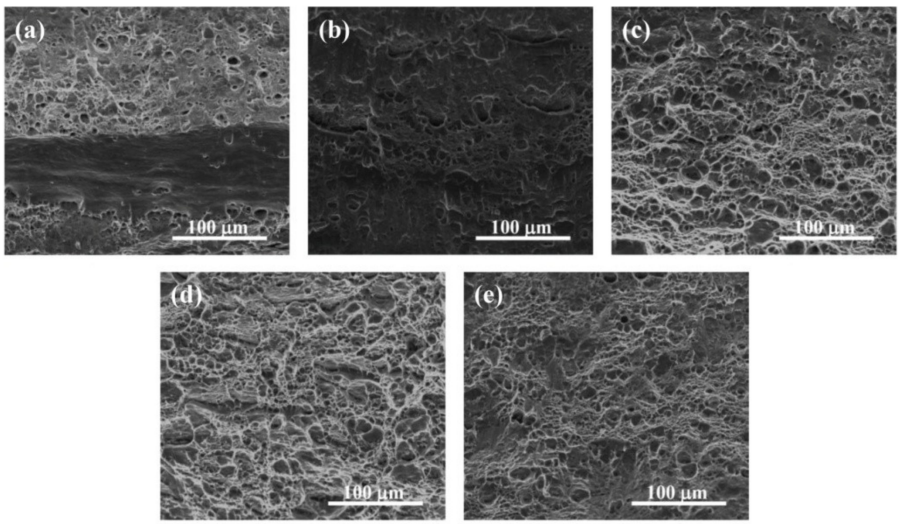

Figure 8. Tensile fracture morphologies of the strips with different Si contents: (**a**) 0.7 wt% Si; (**b**) 0.9 wt% Si; (**c**) 1.1 wt% Si; (**d**) 1.3 wt% Si; (**e**) 1.5 wt% Si.

4. Discussion

4.1. Solute Gradient and Inhomogeneous Deformation

The main cause of the inhomogeneous structure and performance of the VTRC strip is the inhomogeneous solute distribution. The reasons for the negative solute concentration from the surface to the core of the strip include the following three points: First, the surface area of the strip cools at a high rate during the TRC process, significantly increasing the solid solubility of Si. At the same time, the surface low-pressure zone and surface remelting can cause the melt to flow to the surface again and increase the solute concentration [27]. Second, columnar crystals with high aspect ratios were not observed. Figure 9 shows the grain morphology of the VTRC strip with 1.1 wt% Si. Due to the strong self-stirring effect and high cooling rate, the grain growth along the normal direction (ND) is limited by the large number of generated grains, and its morphology is close to equiaxed. The gaps between equiaxed grains are more tortuous and provide strong resistance for the high-solute liquid to be pushed to the middle of the strip. However, this factor can only reduce the solute concentration in the core region of strips to some extent. Third, the drift grain deposition phenomenon unique to vertical casting can clearly reduce the element content in the middle of strips [28]. Drifting grains with low solute concentration were separated from the solidifying front and piled toward the core of the strip under the influence of gravity and the molten pool flow field, completely breaking the solute distribution trend of conventional directional solidification, resulting in the inverse segregation of TRC strips.

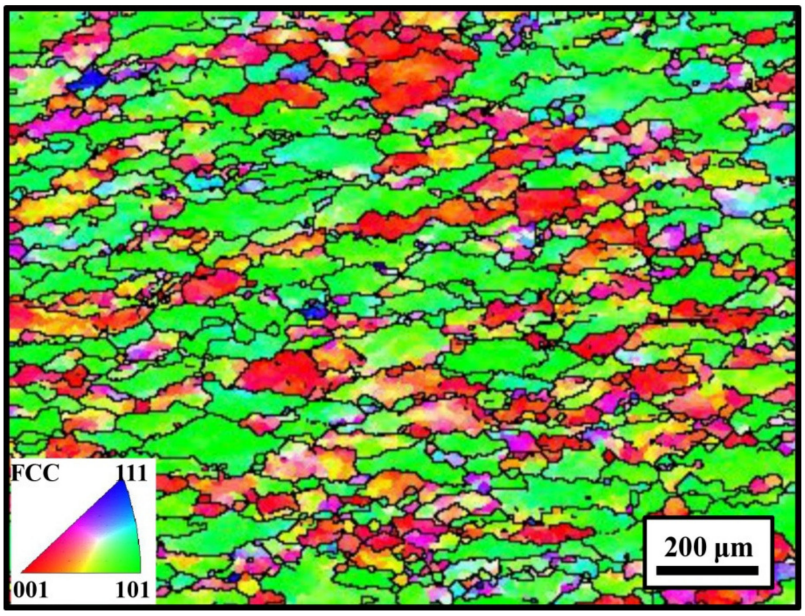

Figure 9. Grain morphology in the 1/4 thickness region of the TRC strip with the content of 1.1 wt% Si.

In addition, the lowest solute concentration in the strip was not found in the centerline region. As can be seen from the element distribution results in Figure 4, an area with a high content of solute elements often appears on either side of the centerline of the strip, which is actually a small-scale solute aggregation. The segregation is different from the macroscopic segregation mentioned above, which is formed by the flow of melt between the grains late in the solidification process. The formation process is divided into three stages, as shown in Figure 10. The gray, orange, blue, and orange arrows in the figure represent the solidified grains, melt, pressure direction, and melt flow direction, respectively. In stage 1, the melt containing a large number of solidified grains was concentrated in the middle region and behaved as a non-Newtonian fluid under stress. During deformation, the intercrystalline gap increases due to the sliding of the grains, leading to Reynolds dilatancy, as shown in stage 2. To compensate for the negative pressure formed by the new gap, the surrounding

fluid is sucked into the middle region, where the solute concentration increases to generate positive segregation (PS), whereas the solute concentration in the surrounding regions decreases to generate negative segregation (NS), as shown in Figure 4. The regions with NS were the EBRs mentioned above. With the increased deformation in stage 3, some grains completely fit together, the gaps of other grains continued to increase, and the surrounding liquid was completely absorbed, finally forming the PS and NS regions that appeared as an intermittent linear segregation band on the macro. Since the segregation region is discontinuous in the RD, line scanning by EPMA along the ND may not cover the PS region. For example, the Mg element of the sample with 1.1 wt% Si in Figure 4 does not show the peak value of Mg in the middle region.

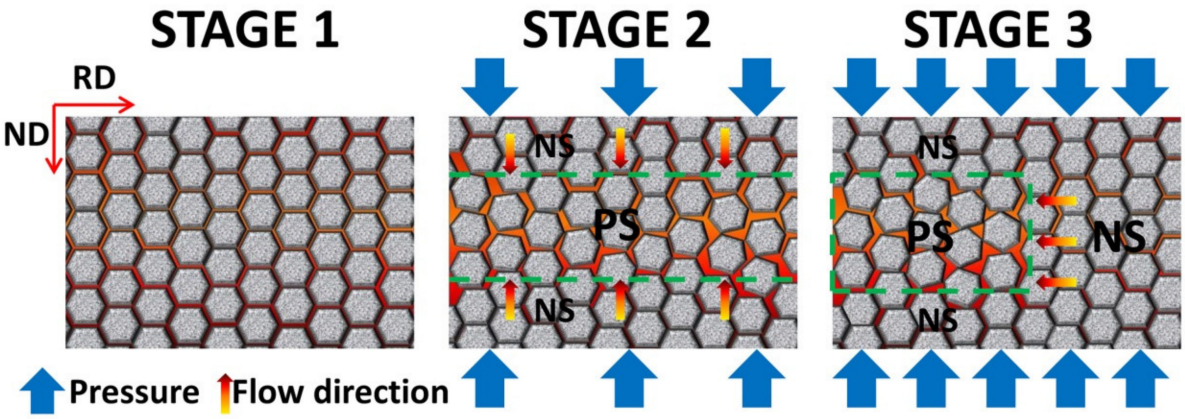

Figure 10. Formation process of local segregation in strips.

Solute gradient is the direct cause of the hardness gradient in the VTRC strip. The hardening degree of T4P alloy mainly depends on the cluster density in the Al matrix. Under the same heat treatment process, the cluster density is mainly affected by the concentration of dissolved solute elements. Therefore, a strip surface with a higher solute concentration has a higher hardening rate during T4P treatment, leading to the soft core characteristics of the hard shell. In the pre-stain process, the core deformation occurs first because of the significant difference in the sliding resistance between the surface and the core of the strip. With the increase in the work-hardening degree of the core, the surface area gradually begins to deform.

4.2. Effect of Si on the Inhomogeneous Deformation in TRC Alloy

In the present study, with the increase in the Si content, the strength and uniform elongation of the TRC strip in the T4P state increased simultaneously, which does not conform to our traditional understanding [11,21,29]. The mechanical properties of Al-Mg-Si alloys are mainly affected by recrystallization, the second phase, and soluble elements [12,30,31]. The relationship between the properties and the structure of the TRC strips was studied in terms of these phenomena.

After solution treatment, the recrystallization grain size was related to the original grain size, recrystallization nucleation, growth rate, and growth time. Due to the short time and low temperature of the aging treatment, no obvious precipitation was found in all samples. Additionally, the heat treatment process was the same for all samples, so there was little difference in the growth rate and growth time of the grains. In this study, the size of the recrystallized grain was determined by the size of the original grain before recrystallization and nucleation. The grain morphology of the TRC and homogenized samples were characterized, as shown in Figure 11. It was found that the grain size difference between the surface and the centerline area of TRC samples is not large. The homogenization process increases the grain size difference between the surface and centerline area, as shown in Figure 11c,d. Due to the high solute concentration on the surface, the insoluble second

phase after homogenization has a greater quantity, which limits the growth of grains during homogenization. The promotion of recrystallization nucleation by micron-sized particles is well documented [32,33]. A large number of Si particles can promote the formation of recrystallized crystal nuclei in a short time, which can reduce the recrystallized grain size, such as the surface of the samples in the T4P state. When the concentration of Si decreases gradually, the Si particles become more dispersed. The deformation around Si particles is more intense, and nucleation is preferred. Compared with regions with more Si particles, grains in regions with fewer Si particles can absorb more regions with high deformation energy to allow grains to grow larger, as exemplified in the central region of samples with 1.1 wt% Si and 1.5 wt% Si. When Si particles are fine and the number of Si particles is small, the promoting effect of particles on nucleation almost disappears, and the recrystallization nucleation is relatively uniform despite the lag, which means that the size of recrystallization does not increase excessively, as demonstrated in the centerline region of the sample with 0.7 wt% Si. However, the Hall–Petch coefficient of Al is small [34], and the size difference in the samples in the present study is not large enough to lead to a significant change in the performance.

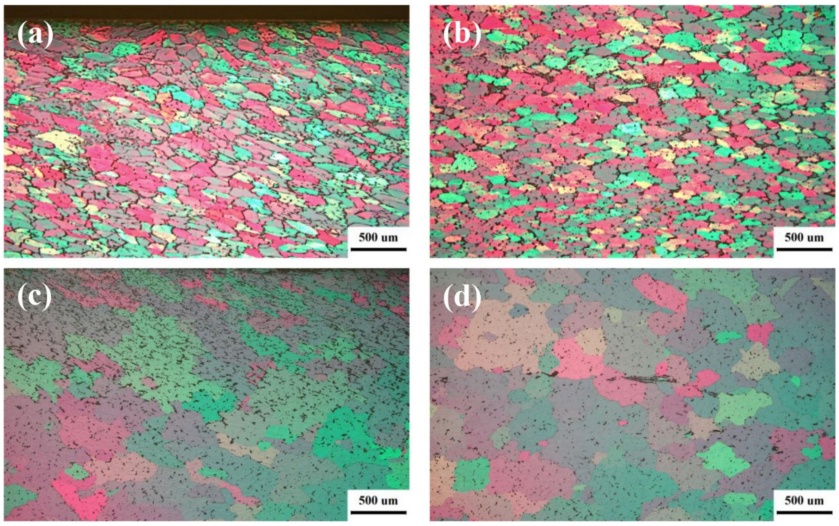

Figure 11. Grain morphology in the surface (**a**) and centerline (**b**) of TRC strips and in the surface (**c**) and centerline (**d**) of homogenized TRC strips with the content of 1.1 wt% Si.

Precipitation at the nanometer level was characterized using TEM. Only the α-Al(Mn, Fe)Si phase and small amount of β′ phase formed during homogenization were found in the grains, and no β″ phase was observed. The precipitates had little effect on the mechanical properties of the alloys. Recent studies have found that cluster strengthening and solution strengthening are the main strengthening modes of Al-Mg-Si alloys in the T4P state, among which cluster strengthening may play a greater role [35]. Increasing Si contents can promote the formation of clusters, and thus improve the strength of the strip, but does not greatly improve the ductility of the strip. At the same time, increasing Si content will increase the number and size of insoluble Si particles. These Si particles can cut the Al matrix and reduce the ductility of the strip. In the Al-Mg-Si alloys with 0.63 wt% Mg prepared by DC, when the Si content was increased to 0.75 wt%, the ductility of the alloy was found to decrease [11]. However, a better strength and ductility of VTRC strip were obtained with the increase in Si content in a larger range.

The inhomogeneous deformation in a strip with low Si content limits the full performance of alloy. As the region with the lowest solute concentration, the EBR region has the slowest work-hardening rate, which will lead to excessive slip in this region and accelerate the formation of initial cracks. Figure 5 shows an obvious premature local deformation in the middle of the sample with 0.7 wt% Si, and a large range of slip will be generated.

The tensile fracture image of the sample also demonstrates the presence of a large SSP in the middle region, as shown in Figure 8. Increasing the work-hardening capacity of ERRs can inhibit premature crack formation. The uniform plastic deformation section of the true stress and true strain curve was determined, and the derivative of the polynomial fitting was used to obtain the work-hardening response curve that reflects the relationship between the instantaneous hardening rate θ and the flow stress σ in the strips with different Si content, as shown in Figure 12. The increase in the Si content significantly improved the work-hardening ability of the strip. When local strong deformation occurs, the strength of the area will also increase rapidly, such that the deformation will be transferred to other low-strength areas, and the degree of inhomogeneous deformation will be decreased. Both strength and uniform elongation are improved with an increase in Si content from 0.7 wt% to 1.1 wt%. Analysis of the EPMA data shows that increasing the amount of added Si can not only supplement the element content in EBRs but also improve the element distribution uniformity. Along the thickness direction, a range of 100 μm above and below the lowest position of Si content was selected, and the ratios of the maximum and minimum contents were compared. When the Si content increased from 0.7 wt% to 1.1 wt%, the ratio decreased from 1.265 to 1.06, indicating that a more uniform element distribution in EBRs was obtained.

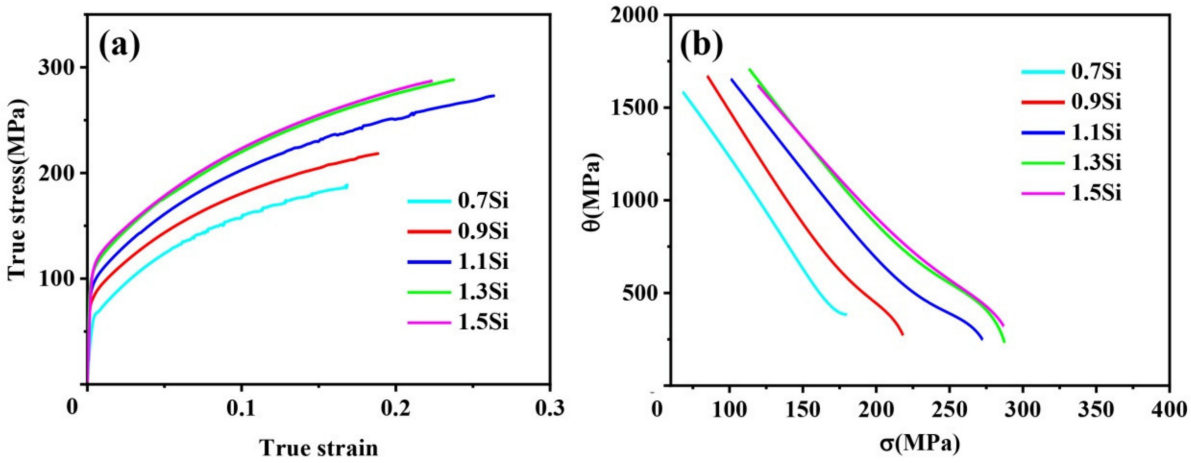

Figure 12. True stress–strain curves (**a**) and work-hardening response curves (**b**) from the tension test of the TRC strips.

When the Si content continued to increase to 1.3 wt%, the work-hardening rate of the alloy continued to increase, but the uniform elongation began to decrease. This indicates that inhomogeneous deformation is no longer the main factor affecting the fracture of the alloy. With an increase in the Si content, the number of insoluble Si particles remaining at the GB increased significantly. Previous studies have shown that these residual Si particles have a negative effect on ductility [11]. However, this adverse effect was not observed when the Si content increased from 0.7 wt% to 1.1 wt%. This is due to the inhomogeneous deformation of the TRC strip. It has been proven that TRC strips with hard shells and soft cores exhibit better ductility than DC strips. The soft structure of the core can withstand greater plastic deformation during the initial stage of deformation. The surface hard shell exhibits a small deformation and limits the expansion of the cracks formed in the core of the strips [36]. The insoluble Si particles were mainly distributed in the hard-surface region. These hard particles did not become the initial crack source because of the small deformation. However, it is clear that the core structure of the strip provides only limited benefits. The number and size of insoluble Si particles increased significantly when the Si content was increased above 1.3%, resulting in them being the main factor limiting the ductility of the strip.

5. Conclusion

The effects of Si on the second phase, recrystallization, and solute gradient of an Al-Mg-Si alloy prepared by sub-rapid solidification TRC were studied. The origins of the limited mechanical properties were also examined. The strength and uniform elongation of the strip were effectively improved by adjusting the Si content. The conclusions are as follows.

1. Sub-rapid solidification and simultaneous deformation provide favorable conditions for the formation of Al-Mg2Si-Si ternary eutectic phases in large quantities during TRC. The ternary eutectic phase increased significantly with increasing Si addition and was difficult to dissolve completely after homogenization. The Si particles formed at the grain boundaries;
2. The Si particles were mainly distributed in the surface region of the strip, due to the negative solute gradient in the thickness direction of TRC strip. The deformation of the TRC strip was inhomogeneous, and the surface area deformation was small during the tensile process, reducing the negative effect of the Si particles on the mechanical properties of the strip. Compared with a DC ingot, a greater amount of Si can be added to a VTRC strip without reducing elongation;
3. The TRC strip is a material consisting of a hard shell and soft core, and the soft core bears the earliest deformation. Premature local deformation in the EBR is the main factor limiting the mechanical properties. With the increase in the Si content from 0.7 wt% to 1.1 wt%, the element content and distribution uniformity in EBR are improved, resulting in a higher work-hardening capability, and inhomogeneous deformation is weakened. The tensile strength and uniform elongation of the strip are increased from 159.44 MPa and 18.36% to 209.96 MPa and 29.791%, respectively.

Author Contributions: Conceptualization, B.W.; methodology, B.W., S.L. and T.J.; validation, G.X., Y.L. and Z.W.; formal analysis, B.W.; investigation, B.W., S.L., T.J. and Y.Z.; resources, G.X. and Y.L.; writing—original draft preparation, B.W.; writing—review and editing, B.W.; funding acquisition, G.X., Y.L. and Z.W. All authors have read and agreed to the published version of the manuscript.

Funding: This study was supported by the National Natural Science Foundation of China (Grant No. 51790485).

Institutional Review Board Statement: Not applicable.

Informed Consent Statement: Not applicable.

Data Availability Statement: Data supporting the reported results can be obtained from the author upon request.

Acknowledgments: The authors acknowledge the Key Laboratory of Electromagnetic Processing of Materials of Ministry of Education and the State Key Laboratory of Rolling and Automation of Northeastern University for assistance in material preparation and analysis.

Conflicts of Interest: The authors declare no conflict of interest.

References

1. Van Huis, M.A.; Chen, J.H.; Sluiter, M.H.F.; Zandbergen, H.W. Phase stability and structural features of matrix-embedded hardening precipitates in Al–Mg–Si alloys in the early stages of evolution. *Acta Mater.* **2007**, *55*, 2183–2199. [CrossRef]
2. Esmaeili, S.; Wang, X.; Lloyd, D.J.; Poole, W.J. On the precipitation-hardening behavior of the Al-Mg-Si-Cu alloy AA6111. *Metall. Mater. Trans. A* **2003**, *34*, 751–763.
3. Yun, M.; Lokyer, S.; Hunt, J.D. Twin roll casting of aluminium alloys. *Mater. Sci. Eng. A* **2000**, *280*, 116–123. [CrossRef]
4. Birol, Y. Analysis of macro segregation in twin-roll cast aluminium strips via solidification curves. *J. Alloys Compd.* **2009**, *486*, 168–172. [CrossRef]
5. Šlapáková, M.; Zimina, M.; Zaunschirm, S.; Kastner, J.; Bajer, J.; Cieslar, M. 3D analysis of macrosegregation in twin-roll cast AA3003 alloy. *Mater. Charact.* **2016**, *118*, 44–49. [CrossRef]
6. Haga, S.S.T. A high speed twin roll caster for aluminum alloy strip. *J. Mater. Process. Technol.* **2001**, *113*, 291–295. [CrossRef]

7. Sun, K.M.; Li, L.; Chen, S.D.; Xu, G.M.; Chen, G.; Misra, R.D.K.; Zhang, G. A new approach to control centerline macrosegregation in Al-Mg-Si alloys during twin roll continuous casting. *Mater. Lett.* **2017**, *190*, 205–208. [CrossRef]
8. Shiju, L.; Jiang, T.; Wang, J.; Chen, L.; Wei, B.; Li, Y.; Xu, G.; Wang, Z. Effects of different external fields on the microstructure and mechanical properties of novel Al Cu Li alloy during twin-roll casting. *Mater. Sci. Eng. A* **2019**, *757*, 14–22. [CrossRef]
9. He, C.; Li, Y.; Li, J.; Xu, G.; Wang, Z.; Wu, D. Effect of electromagnetic fields on microstructure and mechanical properties of sub-rapid solidification-processed Al–Mg–Si alloy during twin-roll casting. *Mater. Sci. Eng. A* **2019**, *766*, 138328. [CrossRef]
10. Jiang, S.; Wang, R. Grain size-dependent Mg/Si ratio effect on the microstructure and mechanical/electrical properties of Al-Mg-Si-Sc alloys. *J. Mater. Sci. Technol.* **2019**, *35*, 1354–1363. [CrossRef]
11. Aucote, J.; Evans, D.W. Effects of excess silicon addition. on ductility of AL-0.95%M92Si alloy. *Met. Sci.* **1978**, *12*, 57–63. [CrossRef]
12. Remøe, M.S.; Marthinsen, K.; Westermann, I.; Pedersen, K.; Røyset, J.; Marioara, C. The effect of alloying elements on the ductility of Al-Mg-Si alloys. *Mater. Sci. Eng. A* **2017**, *693*, 60–72. [CrossRef]
13. Liu, Z.T.; Wang, C.; Luo, Q.; You, J.; Zhou, X.L.; Xu, J.; Mo, Y.T.; Song, J.W.; Zha, M.; Wang, H.Y. Effects of Mg contents on the microstructure evolution and Fe–bearing phase selection of Al–Mg–Si–Fe alloys under sub–rapid solidification. *Materialia* **2020**, *13*, 100850. [CrossRef]
14. Liu, X.; Wang, C.; Zhang, S.-Y.; Song, J.-W.; Zhou, X.-L.; Zha, M.; Wang, H.-Y. Fe-bearing phase formation, microstructure evolution, and mechanical properties of Al-Mg-Si-Fe alloy fabricated by the twin-roll casting process. *J. Alloys Compd.* **2021**, *886*, 161202. [CrossRef]
15. Wang, X.; Ma, P.-K.; Meng, Z.-Y.; Zhang, S.-Y.; Liu, X.; Wang, C.; Wang, H.-Y. Effect of trace Cr alloying on centerline segregations in sub-rapid solidified Al–Mg–Si (AA6061) alloys fabricated by twin-roll casting. *Mater. Sci. Eng. A* **2021**, *825*, 141896. [CrossRef]
16. Engler, O.; Miller-Jupp, S. Control of second-phase particles in the Al-Mg-Mn alloy AA 5083. *J. Alloys Compd.* **2016**, *689*, 998–1010. [CrossRef]
17. Kumar, S.; O'Reilly, K.A.Q. Influence of Al grain structure on Fe bearing intermetallics during DC casting of an Al-Mg-Si alloy. *Mater. Charact.* **2016**, *120*, 311–322. [CrossRef]
18. Park, Y.S.; Lee, S.B.; Kim, N.J. Microstructure and Mechanical Properties of Strip Cast Al-Mg-Si-X Alloys. *Mater. Trans.* **2003**, *44*, 2617–2624.
19. Ji, Y.-L.; Guo, F.-A.; Pan, Y.-F. Microstructural characteristics and paint-bake response of Al-Mg-Si-Cu alloy. *Trans. Nonferrous Met. Soc. China* **2008**, *18*, 126–131. [CrossRef]
20. Lodgaard, N.R.L. Precipitation of dispersoids containing Mn and/or Cr in Al–Mg–Si alloys. *Mater. Sci. Eng. A* **2000**, *283*, 144–152. [CrossRef]
21. Li, Z.; Zhao, P.; Jia, Z.; Liu, Z.; Xie, Z. Effects of Mg and Si contents on the microstructure and mechanical properties of AA6014 alloys in T4P and T6P temper. *Mater. Sci. Eng. A* **2019**, *740–741*, 187–200. [CrossRef]
22. Liu, Y.L.; Kang, S.B.; Kim, H.W. The complex microstructures in an as-cast Al–Mg–Si alloy. *Mater. Lett.* **1999**, *41*, 267–272. [CrossRef]
23. Grydin, O.; Stolbchenko, M.; Nürnberger, F.; Schaper, M. Influence of the twin-roll casting parameters on the microsegregation in thin strips of the aluminium alloy EN AW-6082. *Light Met.* **2014**, *2014*, 411–414.
24. Liu, X.; Zhao, Q.; Ji, Z.; Wang, B.; Zhu, Y.; Jiang, Q. Effectively mitigated macro-segregation and improved tensile properties of twin-roll casting Al-Cu strips via the addition of TiC nanoparticles. *J. Mater. Process. Technol.* **2021**, *296*, 117200. [CrossRef]
25. Kim, M.-S.; Kim, S.-H.; Kim, H.-W. Deformation-induced center segregation in twin-roll cast high-Mg Al–Mg strips. *Scr. Mater.* **2018**, *152*, 69–73. [CrossRef]
26. Wei, B.; Li, S.; Jiang, T.; Xu, G.; Li, Y.; Wang, Z. Effect of a novel semi-solid middle-layer structure formed during twin-roll casting on the mechanical properties of AA6022 alloy. *Mater. Sci. Eng. A* **2021**, *812*, 141083. [CrossRef]
27. Forbord, B.; Andersson, B.; Ingvaldsen, F.; Austevik, O.; Horst, J.A.; Skauvik, I. The formation of surface segregates during twin roll casting of aluminium alloys. *Mater. Sci. Eng. A* **2006**, *415*, 12–20. [CrossRef]
28. Eskin, D.G.; Zuidema, J.; Savran, V.I.; Katgerman, L. Structure formation and macro segregation under different process conditions during DC casting. *Mater. Sci. Eng. A* **2004**, *384*, 232–244. [CrossRef]
29. Hirth, S.M.; Marshall, G.J.; Court, S.A.; Lloyd, D.J. Effects of Si on the aging behaviour and formability of aluminium. *Mater. Sci. Eng. A* **2001**, *319–321*, 452–456. [CrossRef]
30. Onurlu, A.T.S. Effect of heat treatment on the insoluble intermetallic phases present in an AA 6063 alloy. *J. Mater. Sci.* **1994**, *29*, 1652–1655. [CrossRef]
31. Wang, Y.; Deng, Y.; Dai, Q.; Jiang, K.; Chen, J.; Guo, X. Microstructures and strengthening mechanisms of high Fe containing Al–Mg–Si–Mn–Fe alloys with Mg, Si and Mn modified. *Mater. Sci. Eng. A* **2021**, *803*, 140477. [CrossRef]
32. Sidor, J.J.; Decroos, K.; Petrov, R.H.; Kestens, L.A.I. Evolution of recrystallization textures in particle containing Al alloys after various rolling reductions: Experimental study and modeling. *Int. J. Plast.* **2015**, *66*, 119–137. [CrossRef]
33. Engler, O.; Kong, X.W.; Yang, P. Influence of particles stimulated nucleation on the recrystallization textures in cold deformed Al-alloys Part I-experimental observations. *Scr. Mater.* **1997**, *37*, 1665–1674. [CrossRef]
34. Liu, Z.-T.; Wang, B.-Y.; Wang, C.; Zha, M.; Liu, G.-J.; Yang, Z.-Z.; Wang, J.-G.; Li, J.-H.; Wang, H.-Y. Microstructure and mechanical properties of Al-Mg-Si alloy fabricated by a short process based on sub-rapid solidification. *J. Mater. Sci. Technol.* **2020**, *41*, 178–186. [CrossRef]

35. Liu, G.; Zhang, P.; Yang, C.; Zhang, J.; Sun, J. Aluminum Alloys: Solute Atom Clusters and Their Strengthening. *Jinshu Xuebao Acta Metall. Sin.* **2021**, *57*, 1484–1498.
36. Zhao, X.L.; Kuang, J.; Shi, K.K.; Zhang, P.; Xue, H.; Zhang, J.Y.; Liu, G.; Sun, J.; Xu, G.M.; Wang, Z.D. Heterogeneous microstructure-mediated ductile fracture of twin-roll cast Al–Mn strip. *Mater. Sci. Eng. A* **2020**, *783*, 139222. [CrossRef]